Analysis of Petal Rotation Trajectory Characteristics

Rodney L. Anderson*

Jet Propulsion Laboratory, California Institute of Technology, Pasadena, CA 91109, USA

Stefano Campagnola†

Institute of Space and Astronautical Science, Japan Aerospace Exploration Agency, Japan

Brent B. Buffington*

Jet Propulsion Laboratory, California Institute of Technology, Pasadena, CA 91109, USA

In this study, the characteristics of petal rotation trajectories are explored in both the two-body and circular restricted three-body problem (CRTBP) models. Petal rotation trajectories alternate long and short period non-resonant transfers between one or more gravity assist bodies to rotate the line of apsides relative to the central body. They are typically computed using the patched-conic model, and they have been or plan to be used in a number of different missions and mission concepts including Cassini, JUICE, and Europa missions. Petal rotation trajectories are first analyzed here using the patched-conic model to quantify their characteristics and search for cases with fast rotation of the line of apsides. When they are computed in the CRTBP, they are unstable periodic orbits with corresponding stable and unstable manifolds. The characteristics of these orbits are explored from a dynamical systems perspective in the second phase of the study.

I.   Introduction

Petal rotation trajectories alternate long and short non-resonant transfers between one or more gravity assist bodies to rotate the line of apsides relative to the central body. In designing a gravity assist tour, various techniques are used (separately and/or together) to manipulate the spacecraft's orbit geometry relative to the central body including pumping (changing the size of an orbit) or cranking (altering the inclination). Petal rotation trajectories can be used when a change in the orientation of the line of apsides of the spacecraft's orbit is desired. They are typically computed using the patched-conic model assuming a circular orbit for the moon or planet. They have been used for a number of applications including trajectory design with Cassini,[1–5] Europa Missions,[6–8] Neptune-Triton missions,[9,10] JUpiter Icy moon Explorer (JUICE),[11,12] and cycler trajectory concepts.[13] Petal trajectories may also be studied in the circular restricted three-body problem (CRTBP), where they are in fact periodic orbits. In comparison to resonant orbits, the period of these orbits no longer forms an integer ratio with the moon or planet's period of interest, and the difference in the period also affects the rotation of the line of apsides in the inertial frame. Given that the orbit periods no longer form an integer ratio, the orbits are designated using an integer relationship and a superscript with the notation $m{:}n^{\pm}$ $(m, n \in \mathbb{N})$ where m refers to the number of spacecraft revolutions, and n refers to the number of revolutions of the gravity assist body. (Note that the $m{:}n$ notation[14–17] is used here, but the reverse $n{:}m$ notation[18] may also be found in the literature.) The $+$ or $-$ is used to indicate whether the spacecraft revolves more or less than m times and the secondary revolves more or less than n times around the primary in the inertial frame. The special case of alternating $n{:}n^{\pm}$ and $m{:}m^{\mp}$ orbits is particularly interesting and requires the CRTBP model to analyze fully. Each case is designated as a family of $k{:}k$ periodic orbits where $k = m + n$.

---

*Member of Technical Staff, Jet Propulsion Laboratory, California Institute of Technology, 4800 Oak Grove Drive, M/S 301-121, Pasadena, CA 91109, AIAA Senior Member.

†International Top Young Fellow, Institute of Space and Astronautical Science, Japan Aerospace Exploration Agency, AIAA Member.

American Institute of Aeronautics and Astronautics

In the first portion of the study, a parametric analysis is performed using different systems and across multiple resonances with a particular emphasis on missions at Europa, Ganymede, Callisto, and Titan. Specifically, patched-conic techniques are used to compute families of "petals" for different resonances, V_∞ values, and flyby bodies, and a search is made for the cases that give the maximum rotation of the line of apsides per unit time. The ability to rotate the lines of apsides as a function of time is also quantified for each scenario, and particular cases are examined in more detail. Specific $n{:}n^{\pm}/m{:}m^{\mp}$ periodic orbits are computed and analyzed using this model as well.

The patched-conic model gives a good approximation to the actual conditions in the CRTBP for many cases, although limitations do exist for cases where the flybys are distant. The patched-conic model has previously been used to generate initial conditions to study trajectories transitioning between resonances in Anderson and Lo.[17] In the second part of the study, petal rotation trajectories are computed in the CRTBP to examine their characteristics compared to the patched-conic predictions and explore the limitations of the approximation. Given the initial conditions, a multiple shooting method is used to converge these orbits to periodic orbits in the CRTBP.[19] The techniques used to examine these orbits are related to those developed in Anderson, Campagnola, and Lantoine[20] exploring resonant orbits. They also possess some interesting characteristics that are similar to these resonant orbits which have been shown to be useful in understanding tour design in the CRTBP.[21–26] Particular two-body cases are evaluated in the CRTBP for the study, and equivalent periodic orbits are computed using the patched conic initial conditions. The rate of change of the line of apsides in the CRTBP is compared to the patched-conic predictions for various cases. The characteristics of these trajectories, such as stability, are also examined and summarized.

II.   Methodology

A.   Resonant Transfers

The focus in this study is on non-resonant transfers, but it is useful to briefly review resonant transfers as a basis for comparison. Resonant transfers have been designed using patched-conic methods for some time, and with these types of resonant transfers in the two-body system, the period of the spacecraft $\mathbb{P}_{s/c}$ may be related to the secondary's period $\mathbb{P}_s$ by
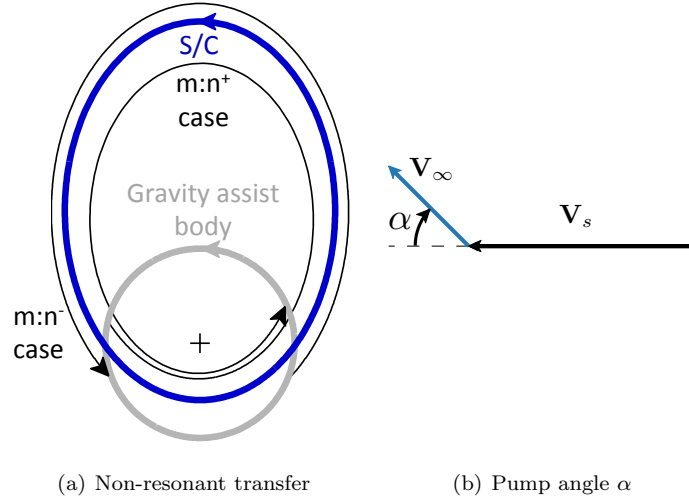
$$\mathbb{P}_{s/c} = \frac{n}{m}\mathbb{P}_s. \tag{1}$$

The spacecraft in the patched-conic model encounters the gravity assist body at the same longitude in each case. A change in the two-body orbit of the spacecraft relative to the central body is effected by rotating the V_∞ vector via a flyby of the spacecraft by the gravity assist body on a hyperbolic trajectory. This technique can also be used to rotate the longitude of the argument of periapse in addition to altering other orbital elements. See Uphoff, Roberts, and Friedman[27] or Strange and Sims[28] for more information on resonant transfers using patched-conic methods, and see Anderson and Lo[21,24] for a description of these transitions from a dynamical systems perspective.

B.   Non-Resonant Transfers

Non-resonant transfers may also be called generic or non-$n\pi$ returns, and in these transfers the spacecraft goes through slightly more or less than m revolutions. They have several characteristics that are different from the resonant transfers. In particular, non-resonant transfers must occur in the orbit plane of the gravity assist body or secondary. The exception to this is the case of π-transfers, which are typically inclined. Again, they are designated using the notation $m{:}n^{\pm}$ where a $+$ indicates a long transfer and a $-$ indicates a short transfer. In the following, an inbound flyby is defined as a flyby that occurs before periapsis of the spacecraft orbit, and an outbound flyby is one that occurs after periapsis. See Figure 1(a) for an illustration of a long and short transfer. The equations for computing the two-body orbits required for the non-resonant transfers may be found in Campagnola, Strange, and Russell[29] or Strange and Sims,[28] but a short overview will be given here. In this formulation, the notation

$$\sigma = \begin{cases} +1 & \textit{short transfer} \\ -1 & \textit{long transfer} \end{cases}$$

American Institute of Aeronautics and Astronautics

(a) Non-resonant transfer   (b) Pump angle α

Figure 1. Illustration of possible non-resonant transfers including possible $m{:}n^+$ and $m{:}n^-$ cases and the pump angle at the flyby.

$$EI = \begin{cases} +1 & \textit{if } n \geq m \\ -1 & \textit{if } n < m \end{cases}$$

is used. An exterior resonance is designated by $EI = 1$, and an interior non-resonance by $EI = -1$. For planar problems with rotation symmetries, an orbit is defined by two parameters. Non-resonant orbits must also satisfy a phasing constraint, so that the boundary positions of the spacecraft match those of the secondary. Then for a choice of m, n and σ, non-resonant orbits belong to a one-dimensional manifold, which is implicitly defined by the phasing constraint. Generally for a given m and n one inbound-outbound and one outbound-inbound transfer exists[28] although exceptions exist at low V_∞.[28]

In this paper, the dimensionless periapse and apoapse radii (r_p and r_a) are chosen as independent variables, following the formulation in Campagnola, Strange, and Russell.[29] Using this formulation the length scale factor is the semimajor axis of the secondary's orbit around the primary $\tilde{a}$, and the time scale factor is $\sqrt{\tilde{a}^3/GM_p}$. In this case, GM_p is the gravitational parameter of the primary, and these factors may be used to convert between dimensional and dimensionless quantities in the patched-conic equations. Using these conversions with the two-body equations, it can be shown that the dimensionless speed of the secondary $V_s = 1$. In the patched-conic model, circular motion is assumed for the secondary which is assumed to be massless, and flybys are modeled as impulsive changes of velocity. Given that the patched-conic formulas in this paper are normalized with the semimajor axis and speed of the secondary, the period of the secondary is 2π, and the mass parameter of the primary is one. This is distinct from the normalization used in the CRTBP where the combined mass of the primary and secondary are one.

The phasing constraint becomes

$$2f_0(r_a, r_p) + [2\pi m - 2M_0(r_a, r_p) + \pi\sigma(1 - EI)]\left(\frac{r_a + r_p}{2}\right)^{3/2} - 2\pi n + \sigma(1 - EI) = 0 \qquad (2)$$

where f_0 is the initial true anomaly

$$f_0(r_a, r_p) \doteq -\sigma EI \arccos\left(\frac{2r_a r_p - r_a - r_p}{r_a - r_p}\right) \qquad (3)$$

and M_0 is the initial mean anomaly

$$M_0(r_a, r_p) \doteq -2\sigma EI\left[\arctan\left(\sqrt{\frac{1 - r_p}{r_a - 1}}\right) - \frac{\sqrt{(r_a - 1)(1 - r_p)}}{r_a + r_p}\right]. \qquad (4)$$

American Institute of Aeronautics and Astronautics

Equation 2 can be solved for a fixed r_p (if $n \geq m$) or r_a (if $n < m$). Although other choices of independent variables are possible,[29] the pericenter-apocenter formulation is convenient because only one solution exists if r_a is fixed (for $n \leq m$) or if r_p is fixed (for $n \geq m$). Given the velocity of the spacecraft ($\mathbf{V}_{s/c}$) and the secondary ($\mathbf{V}_s$) in the inertial frame, the relative velocity in the patched-conic model at the gravity assist encounter is $\mathbf{V}_\infty = \mathbf{V}_{s/c} - \mathbf{V}_s$. Using this notation, a number of quantities may be computed using dimensionless variables including dimensionless V_∞ given by $v_\infty = |\mathbf{v}_\infty|$, the pump angle α, and the time of flight (TOF). They are defined according to

$$v_\infty = \sqrt{3 - \frac{2}{r_a + r_p} - 2h} \qquad (5)$$

$$\alpha = \arccos\left(\frac{h-1}{V_\infty}\right) \qquad (6)$$

$$TOF = [2\pi m - 2M_0(r_a, r_p) + \pi\sigma(1 - EI)]\left(\frac{r_a + r_p}{2}\right)^{3/2} \qquad (7)$$

where $h = 2r_a r_p/(r_a + r_p)$. The pump angle is the angle between the secondary's velocity vector and the V_∞ vector as illustrated in Figure 1(b).[27, 30, 31] Figure 2 shows the pump angles for dimensionless V_∞ values for a variety of resonant, short non-resonant, and long non-resonant cases. The dimensionless V_∞ is simply the dimensional V_∞ normalized by the magnitude of the circular velocity of the secondary. For a given V_∞, the
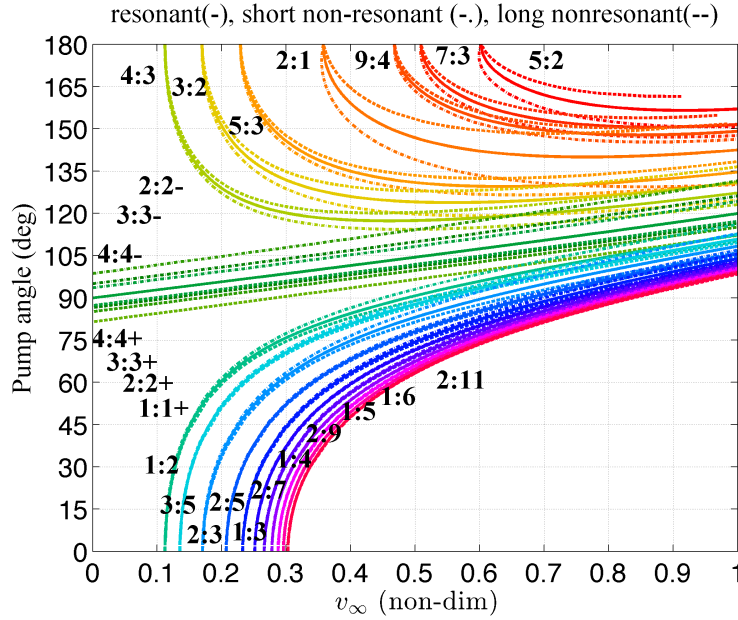

Figure 2. Pump angle across V_∞ for selected resonant and non-resonant orbits.

chart may generally be used in combination with the maximum bending angle achievable for the system of interest to determine whether transferring between two desired resonances is possible. The position vector at closest approach or the periapse relative to the secondary may be computed as

$$\mathbf{r}_{ps} = r_{ps}\frac{\mathbf{V}_\infty^- - \mathbf{V}_\infty^+}{|\mathbf{V}_\infty^- - \mathbf{V}_\infty^+|} \qquad (8)$$

where

$$r_{ps} = \frac{GM_s}{V_\infty^2}\left(\frac{1}{\sin\delta/2} - 1\right). \qquad (9)$$

American Institute of Aeronautics and Astronautics

Here, GM_s is the gravitational parameter of the secondary or gravity assist body, and δ is the bending angle obtained from the rotation of the V_∞ vector. The velocity at closest approach is defined by

$$\mathbf{v}_{ps} = v_{ps} \frac{\mathbf{V}_\infty^+ + \mathbf{V}_\infty^-}{|\mathbf{V}_\infty^+ + \mathbf{V}_\infty^-|} \tag{10}$$

where v_{ps} is computed using the energy of the hyperbolic flyby trajectory around the secondary as

$$v_{ps} = \sqrt{V_\infty^2 + 2GM_s/(r_{ps})}. \tag{11}$$

These equations may be used to compute dimensional or dimensionless quantities by using the appropriate values within the equations. The dimensionless mass parameter for the secondary in this case should be the secondary's dimensional mass parameter normalized by GM_p.

C.   Circular Restricted Three-Body Problem

The CRTBP is used to analyze petal rotation trajectories from a dynamical systems perspective in this study. An overview of the model is given here, and Szebehely[32] may be referred to for more details. In this model, two massive bodies rotate about their barycenter in circular orbits. The larger body is often referred to as the primary and the smaller body is referred to as the secondary. Note that in this paper the secondary will also always be the gravity assist body. The objective is to model the motion of a third infinitesimal mass under the influence of the primary and secondary. The equations of motion are typically made dimensionless so that the mass of the primary is $1 - \mu$ and the mass of the secondary is μ. In the rotating frame, the primary is located on the x axis at $x_1 = -\mu$, and the secondary is located at $x_2 = 1 - \mu$. Given this information, the equations of motion of the infinitesimal mass are written in the rotating frame as

$$\ddot{x} - 2\dot{y} = \frac{\partial \Omega}{\partial x}, \quad \ddot{y} + 2\dot{x} = \frac{\partial \Omega}{\partial y}, \quad \ddot{z} = \frac{\partial \Omega}{\partial z} \tag{12}$$

where

$$\Omega = \frac{x^2 + y^2}{2} + \frac{(1 - \mu)}{r_1} + \frac{\mu}{r_2} \tag{13}$$

and

$$r_1 = \sqrt{(x + \mu)^2 + y^2 + z^2}, \quad r_2 = \sqrt{(x - 1 + \mu)^2 + y^2 + z^2}. \tag{14}$$

The mass ratios of the moons are listed for selected CRTBP systems in Table 1. An integral of motion called

Table 1. Mass ratios for selected CRTBP systems

System	μ	System	μ
Jupiter-Io	4.705093×10^{-5}	Jupiter-Callisto	5.667999×10^{-5}
Jupiter-Europa	2.526645×10^{-5}	Saturn-Titan	2.365805×10^{-4}
Jupiter-Ganymede	7.803691×10^{-5}	Neptune-Triton	2.087757×10^{-4}

the Jacobi constant is found in this problem, and it is defined according to

$$C = x^2 + y^2 + \frac{2(1 - \mu)}{r_1} + \frac{2\mu}{r_2} - \dot{x}^2 - \dot{y}^2 - \dot{z}^2. \tag{15}$$

III.   Patched-Conic Exploration

Petal rotation trajectories as they are referred to here are computed using the non-resonant techniques discussed earlier with the specific objective of rotating the line of apsides. A schematic of one such scenario for the $1{:}4^-/1{:}2^+$ case is shown in Figure 3. In this schematic, the change in the line of apsides as a result of the gravity flybys may be found by examining the orbital elements after the flybys. This change and the rate of change of the argument of periapse may be computed analytically using patched-conic equations as will
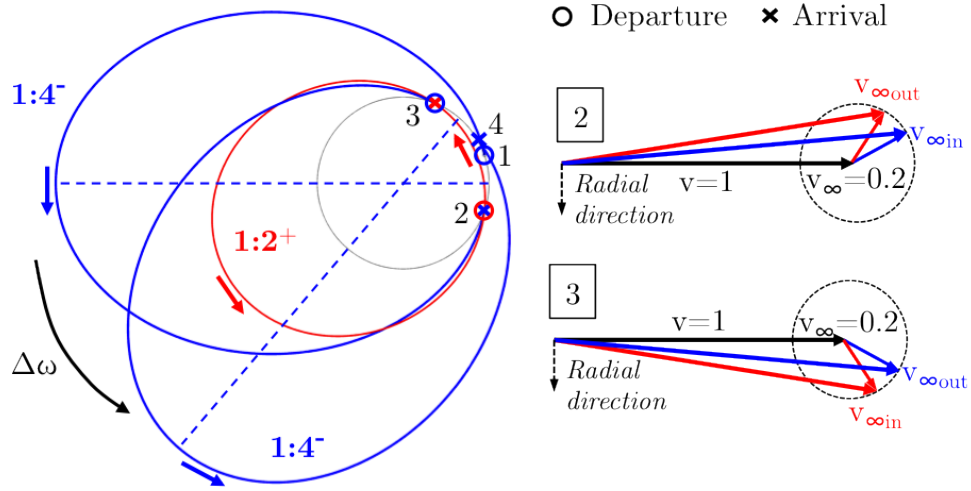
Figure 3. Petal strategy schematic for a $1:4^-/1:2^+$ sequence with the rotation of the line of apsides.

be described next. Practically speaking there are also several other considerations in the design process. To avoid very low altitudes, we assume that, for each flyby, the radial component of the incoming and outgoing V_∞ vectors have the same sign. For instance, the flyby number 2 in Figure 3 shows both the incoming V_∞ vector (belonging to the $1:4^-$ orbit) and the outgoing V_∞ vector (belonging to the $1:2^+$ orbit) with a negative radial component. Note that if we were to replace the $1:2^+$ orbit with a $1:2^-$ orbit, the outgoing V_∞ vector of flyby number 2 would be positive. Then flyby number 2 would require a larger bending angle (and a smaller radius of closest approach) to flip the V_∞ vector.[33] So we typically alternate short orbits to long orbits. More generally, if the first orbit is $m_1 : n_1^{\sigma 1}$ and the second orbit is $m_2 : n_2^{\sigma 2}$, then

$$\sigma_2 = \begin{cases} -\sigma_1 & \text{if} \quad \text{sign}(n_1 : m_1 - 1) = \text{sign}(n_2 : m_2 - 1) \\ \sigma_1 & \text{if} \quad \text{sign}(n_1 : m_1 - 1) \neq \text{sign}(n_2 : m_2 - 1) \end{cases}$$

If α_1 is the pump angle of the first non-resonant orbit, and α_2 is the pump angle of the second non-resonant orbit, the required flyby bending angle is $|\alpha_2 - \alpha_1|$, while the bending or turn angle that can be provided by the flyby is

$$\delta \doteq 2\arcsin\left(\frac{1}{1 + V_\infty^2/V_c^2}\right). \tag{16}$$

Here V_c is the velocity of a circular orbit at the same radius as the flyby closest approach r_{ps} given by

$$V_c = \sqrt{GM_s/r_{ps}}. \tag{17}$$

Note that V_c may also be computed as dimensional or dimensionless by using the appropriate values for the mass parameter and radius. The minimum-altitude flyby constraint results in $V_c \leq V_{cMAX}$, where

$$V_{cMAX} = \sqrt{\frac{GM_s}{r_{body} + h_{min}}}. \tag{18}$$

The radius of the secondary is r_{body} with a minimum acceptable flyby altitude of h_{min}. The values of V_c for different secondaries are shown in Table 2 along with several other parameters of interest. For any (feasible) petal strategy, the rotation of the line of nodes after two flybys may be computed from Equation 7 using the total dimensionless time of flight of the two non-resonant orbits given by

$$\Delta\omega(r_{a1}, r_{p1}) = TOF(r_{a1}, r_{p1}) + TOF(r_{a1}, r_{p1}) - 2\pi(n_1 + n_2). \tag{19}$$

Refer again to Figure 3 to see the rotation of the argument of periapse per revolution of the secondary body given by $\frac{\Delta\omega}{2\pi(n_1+n_2)}$ for an example case.

Table 2. V_{cMAX} **for different systems**

Body	GM (km^3/s^2)	Mean velocity (km/s)	Radius (km)	Flyby altitude (km)	V_{cMAX} $(adim)$
Earth	398659	29.78	6378	300	0.259
Moon	4843.94	1.018	1737	50	1.62
Io	5960.98	17.33	1829	100	0.101
Europa	3200.99	13.74	1564	100	0.101
Ganymede	9887	10.88	2632	100	0.175
Callisto	7180.97	8.203	2409	100	0.206
Enceladus	7.96556	12.62	256.6	50	0.0128
Titan	8978.17	5.572	2575	800	0.293
Triton	1427.92	4.389	1353	300	0.212

Values of $\Delta\omega$ and the rate of change of ω over time ($\dot{\omega}$) may be computed for any particular system and $m{:}n^{\pm}/m{:}n^{\mp}$ combination. The results may be plotted compactly using $\dot{\omega}$ in terms of the degrees per secondary revolution, and the dimensionless V_{∞}. The results for some selected orbits useful in various systems are plotted in Figure 4. In each case the system where the stated $\dot{\omega}$ is possible is indicated by

(a) Overview

(b) Close View
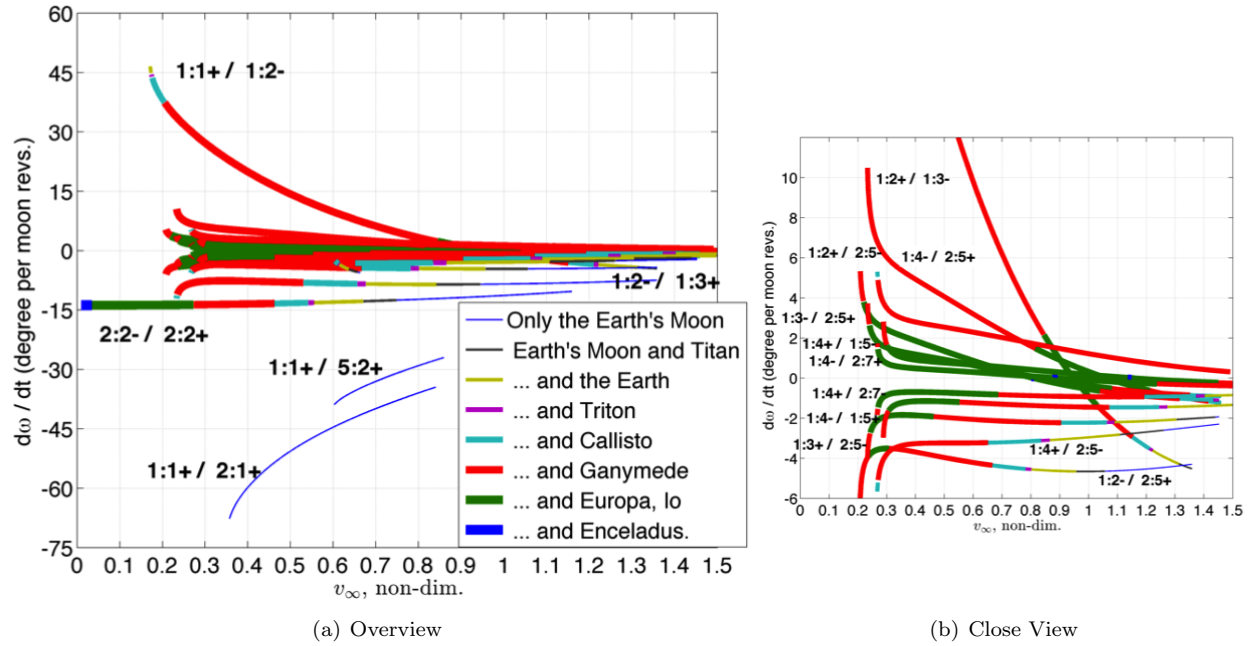
Figure 4. $\dot{\omega}$ **across a range of dimensionless V_{∞} values for a set of non-resonant orbit combinations.**

the color and thickness of the line as indicated in the legend. Note that the colors further down in the list include all of the systems listed above, and those lines are valid for all of the systems listed above that line. The feasibility of each solution is limited by the allowable bending angle given the minimum flyby altitude constraint. In each case, for a given V_{∞}, a range of orbits and $\dot{\omega}$ rates are possible. For many scenarios it is often desirable to maximize $\dot{\omega}$, and in this case the appropriate orbit may be selected from Figure 4 for a given V_{∞}.

While the dimensionless parameters are convenient to visualize a wide range of possibilities in different systems, it is also useful to plot the results for particular systems to more easily find the appropriate orbits. Plotting in this manner allows the possible $\dot{\omega}$ values to be compared for various sequences for a given V_{∞}

American Institute of Aeronautics and Astronautics

in each system. Ideally a mission designer can use this information during the tour to select the desired rotation at the current V_∞ being used in the design. It may also allow for the targeting of a particular V_∞ where a desired rate of $\dot{\omega}$ may be achieved. Some of the selected sequences that have been found to be useful or have the potential to be useful in various system are plotted in Figures 5 and 6. The sequences for the
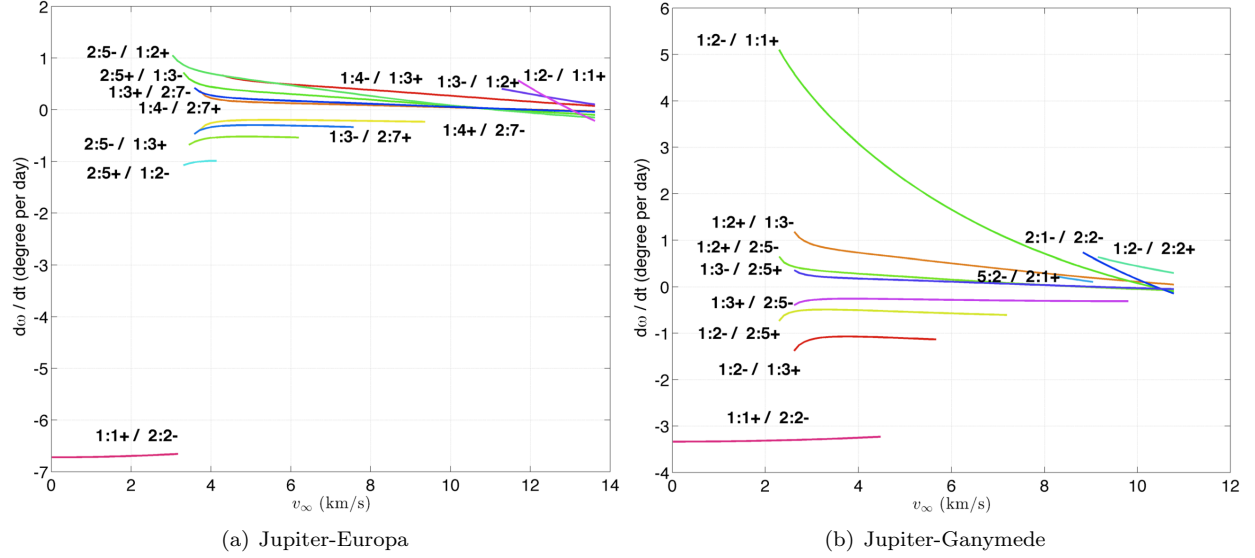

(a) Jupiter-Europa

(b) Jupiter-Ganymede

Figure 5. $\dot{\omega}$ **over** V_∞ **for the Jupiter-Europa and Jupiter-Ganymede dimensional cases.**
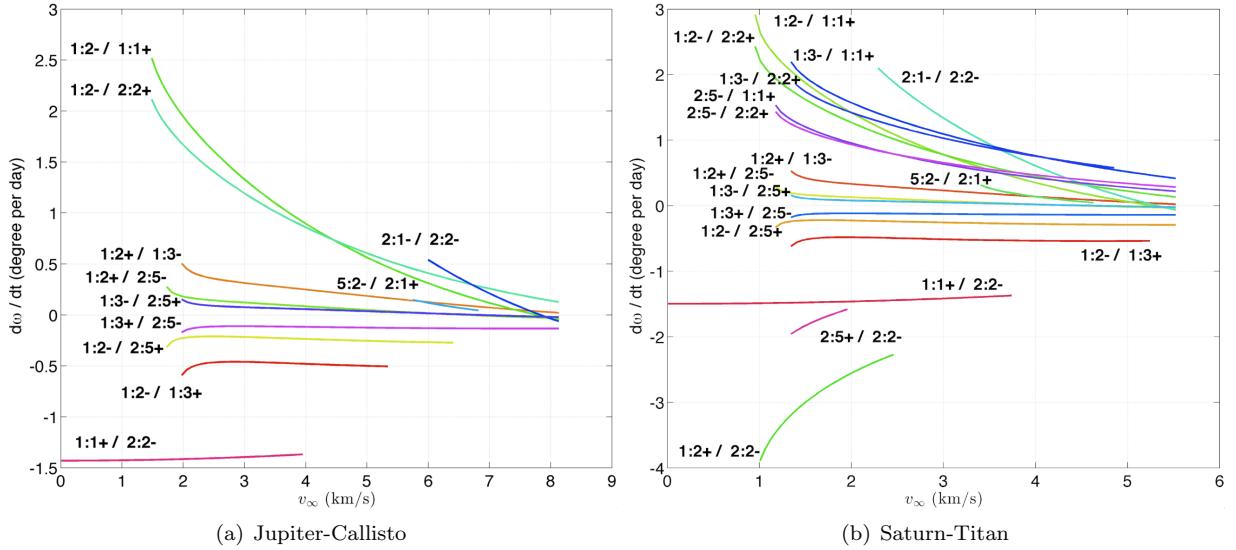

(a) Jupiter-Callisto

(b) Saturn-Titan

Figure 6. $\dot{\omega}$ **over** V_∞ **for the Jupiter-Callisto and Saturn-Titan dimensional cases.**

Jupiter-Europa system in Figure 5(a) have generally been tailored to minimize the effects of radiation on the spacecraft while the other cases are focused more on finding the maximum rotation of the line of apsides. As expected, the $1{:}1^+/2{:}2^-$ case often gives one of the higher rates of $\dot{\omega}$, but it is interesting that the $1{:}2^+/2{:}2^-$ case appears to be quite effective for the Saturn-Titan system. A range of other factors beyond maximizing the rotation of the line of apsides may come into play in the mission design, and these figures allow the proper trades to be made. Note that the $n{:}n^+/m{:}m^-$ orbits will be dealt with more fully in the remainder of the paper, and the validity of the patched-conic predictions at low values of V_∞ will be evaluated.

IV. Transition to the CRTBP

A. Generating the Initial Conditions

A detailed example transitioning from the patched-conic model to the CRTBP using a $1{:}1^+/2{:}2^-$ case in the Jupiter-Europa system is first presented here to describe the process used to compute these orbits. For this case, the initial conditions at the flyby required to travel along the $1{:}1^+$ trajectory with $V_\infty/V_s = 0.232$ are computed. After one flyby, the spacecraft travels along the $1{:}1^+$ orbit, and after the next it travels along the $2{:}2^-$ orbit. The subsequent flyby transfers the spacecraft back to the $1{:}1^+$ orbit, and the cycle repeats. During this time the line of apsides rotates as a result of each flyby.

Using Equations 5 through 10, the initial $\mathbf{V}_\infty$ vectors are computed in the RTN frame. For this case, the $\hat{R}$ direction is the radial direction positive traveling out from the barycenter to the gravity assist body. The $\hat{N}$ direction is the orbit normal, and $\hat{T}$ completes the right hand frame. Given this coordinate system, the $\mathbf{V}_\infty$ pair for one flyby is

$$\mathbf{V}_\infty^{A-} \approx [\ 0.23191 \quad 0.00644\ ]^T \tag{20}$$

$$\mathbf{V}_\infty^{A+} \approx [\ 0.22338 \quad -0.06264\ ]^T \tag{21}$$

where the A in the superscript denotes the flyby. The "–" indicates the incoming $\mathbf{V}_\infty$, and the "+" indicates the outgoing $\mathbf{V}_\infty$. The other flyby's $\mathbf{V}_\infty$ pair is

$$\mathbf{V}_\infty^{B-} \approx [\ -0.22338 \quad -0.06264\ ]^T \tag{22}$$

$$\mathbf{V}_\infty^{B+} \approx [\ -0.23191 \quad 0.00644\ ]^T. \tag{23}$$

After flyby A, the spacecraft enters the $2{:}2^-$ orbit, and after flyby B, it enters the $1{:}1^+$ orbit.

Note that $\mathbf{V}_\infty^{A+}$ and $\mathbf{V}_\infty^{B-}$ do not match because the spacecraft is encountering the gravity assist body at a different location along the gravity assist body's orbit in each case. This feature distinguishes this technique from a resonant encounter where the outgoing and subsequent incoming $\mathbf{V}_\infty$s would be the same.[24] If the outgoing/incoming $\mathbf{V}_\infty$ pairs are examined using the diagram in Figure 7, it can be seen that the velocities are consistent with the expected characteristics for the $1{:}1^+$ and $2{:}2^-$ orbits. Examining flyby A, the outgoing
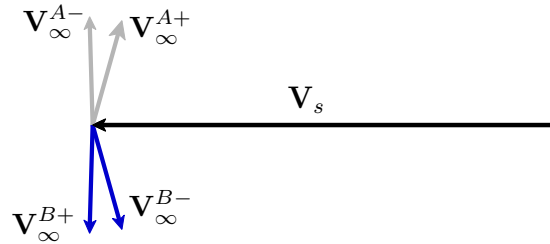

Figure 7. Diagram showing $\mathbf{V}_\infty$ vectors relative to the gravity assist body's velocity.

$\mathbf{V}_\infty^{A+}$ has a positive velocity in the $\hat{R}$ direction and a negative velocity in the $\hat{T}$ direction indicating an outbound trajectory traveling to apoapse on the orbit. The incoming $\mathbf{V}_\infty^{B-}$ has a negative velocity in the $\hat{R}$ and $\hat{T}$ directions which is consistent with an incoming V_∞. The $\mathbf{V}_\infty^{A+}$ and $\mathbf{V}_\infty^{B-}$ pair is also consistent with the $1{:}1^+$ orbit.
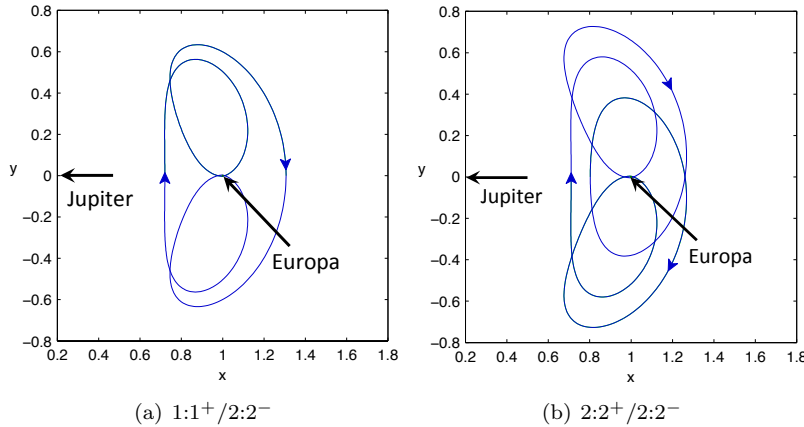
B. Convergence Process in the CRTBP

Once each $\mathbf{V}_\infty$ has been computed using the patched-conic equations, the flyby conditions at closest approach to the gravity assist body may be computed. These initial conditions have been found to be the easiest to use in the CRTBP to converge on the truly periodic orbits approximated by the patched-conic equations. In this process, the closest approach conditions for both flybys are transferred to the CRTBP, and initial guess trajectories are integrated forward and backward from each flyby for half of the expected periods. Examples of two particular cases computed in the Jupiter-Europa system using this process are given in Figure 8. The resulting trajectories appear nearly periodic, but they can have significant discontinuities at the endpoints, especially for lower energies or V_∞ values.

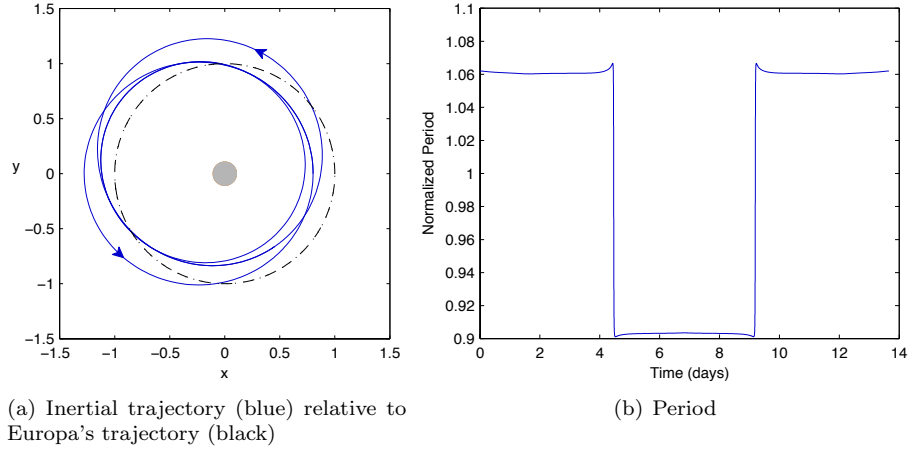(a) 1:1$^+$/2:2$^-$ (b) 2:2$^+$/2:2$^-$
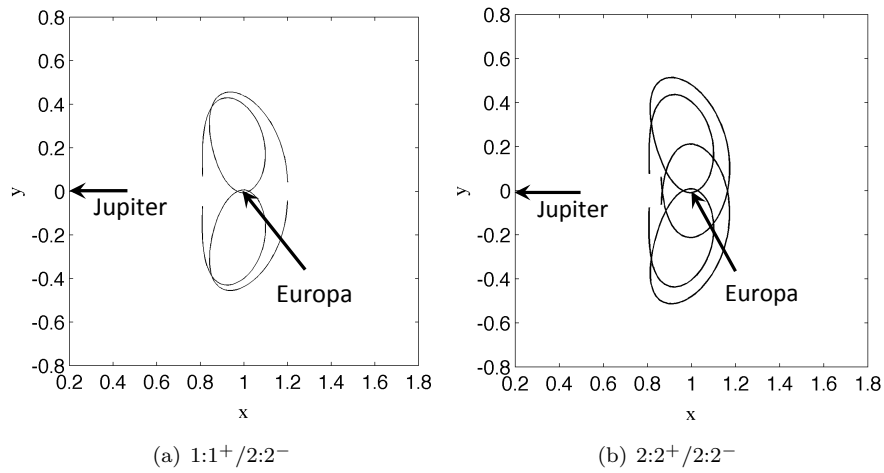
Figure 8. Two orbit cases with two-body initial conditions integrated forward in the CRTBP.

The next step in the process is to use the integrated initial guess trajectories in a differential corrector to compute a periodic trajectory with the same topological characteristics. A two-level differential corrector with periodic constraints is generally used for this purpose,[34–36] although a single-shooting method[37] is sometimes used for the simplest cases. A sample of the orbits corresponding to the initial conditions in Figure 8 are given in Figure 9. As can be seen from the plot, the patched-conic initial conditions provide a

(a) 1:1$^+$/2:2$^-$ (b) 2:2$^+$/2:2$^-$

Figure 9. Converged three-body orbits plotted in the rotating Jupiter-Europa frame.

sufficient approximation to the final converged three-body orbits for these cases. The convergence process does introduce some differences however that make the introduction of other techniques, such as continuation methods, desirable, even for high energy cases. For example, the predicted closest approach at Europa for the example discussed in the previous section was at an altitude of approximately 224 km, but the converged distance was approximately 64 km. These differences are partly the result of the vagaries of the particular method used for the differential corrections process, but it is useful to produce the entire family of periodic orbits as will be discussed next. Orbits in the CRTBP with desired characteristics, such as periapse radius, may then be selected from the family. Examining the orbits that are periodic in the CRTBP in the inertial frame reveals the differences in the two-body orbits before and after the flybys more clearly as seen for the 2:2$^+$/2:2$^-$ in Figure 10(a). The difference in the direction of the argument of periapse can also be discerned and will be explored in more detail later. The difference in the two-body orbits may be clearly seen by plotting characteristics such as the osculating two-body period of the orbit shown in Figure 10(b).
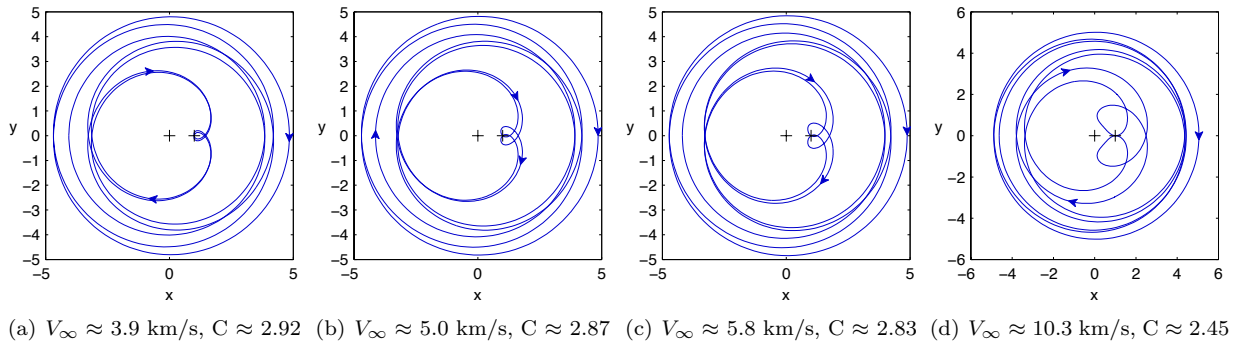
American Institute of Aeronautics and Astronautics

(a) Inertial trajectory (blue) relative to Europa's trajectory (black)

(b) Period

Figure 10. The converged three-body case in Figure 9(b) plotted in the inertial frame with its period normalized by Europa's period over time.

V. Comparison of Patched-Conic and CRTBP Results

It is expected that the patched-conic and CRTBP results will match well for higher energies, and that differences between the results from each model will occur in the low-energy regimes. In order to explore the differences that might occur several example cases relevant to various mission designs are examined. The first is a $1{:}4^+/1{:}5^-$ sequence in the Jupiter-Europa system that is used to minimize radiation exposure. Then an in-depth examination of the $1{:}1^+/2{:}2^-$ case is presented.

### A. Jupiter-Europa $1{:}4^+/1{:}5^-$ Sequence

The $1{:}4^+/1{:}5^-$ sequence is typically used at higher energies to rotate the line of apsides, and it also has the benefit that it can be used to minimize radiation exposure when performing flybys of Europa. This lower radiation exposure is achieved by the fact that it has a high apoapse radius with a periapse very close to Europa's radius. For this process, the methods just described were used to converge an initial guess from the patched-conic model in the CRTBP. Once this initial guess was obtained, the orbit family over a range of Jacobi constants and V_∞ values was obtained using continuation.[38, 39] A sample of the periodic orbits obtained during this process is shown in Figure 11. As can be seen from the plot, the orbit can vary

(a) $V_\infty \approx 3.9$ km/s, C ≈ 2.92 (b) $V_\infty \approx 5.0$ km/s, C ≈ 2.87 (c) $V_\infty \approx 5.8$ km/s, C ≈ 2.83 (d) $V_\infty \approx 10.3$ km/s, C ≈ 2.45

Figure 11. Selected trajectories from the Jupiter-Europa $1{:}4^+/1{:}5^-$ family.

significantly with energy, but the same general qualities expected for the $1{:}4^+/1{:}5^-$ orbit are seen in each plot.

One of the primary characteristics of interest for this study is the rate at which the argument of periapse may be rotated over time for different orbits and values of V_∞. A comparison between predictions using the patched-conic equations and the results from the converged periodic orbit equivalents in the CRTBP are

American Institute of Aeronautics and Astronautics
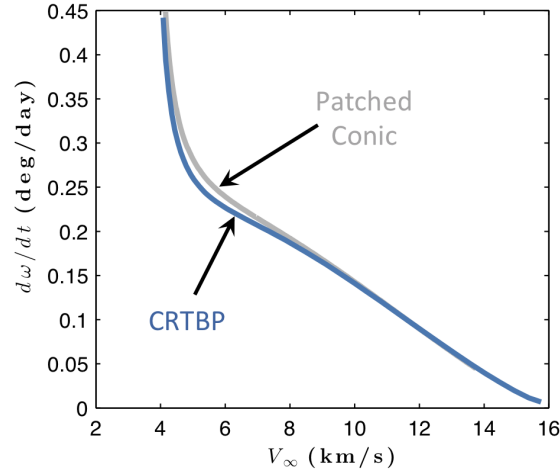
Figure 12. Comparison of the patched-conic $\dot{\omega}$ and the CRTBP $\dot{\omega}$ over a range of V_∞ values for the 1:4$^+$/1:5$^-$ sequence.

shown in Figure 12. It can be seen from the plot that the predicted and computed $\dot{\omega}$ values match quite well for the larger V_∞ values. As the V_∞ values fall below approximately 6 km/s, some differences start to become apparent. This difference occurs despite the fact that the majority of the orbit stays away from the secondary.

B. Jupiter-Europa 1:1$^+$/2:2$^-$ Sequence

As the spacecraft's orbit becomes more similar to the gravity assist body's orbit it is expected that the effect of the gravitational perturbations of the gravity assist body will become more important along the trajectory and more significant differences will be observed when comparing the patched-conic predictions and the CRTBP periodic orbits. One such case may be seen for the orbit following the 1:1$^+$/2:2$^-$ sequence in the Jupiter-Europa system. This case will be examined in more detail here, and relevant information will be summarized for various sequences and systems in the following section.

The initial orbit in this family was computed using the patched-conic initial guess, and the family was then obtained using continuation. A sample of some of the orbits resulting from this process is shown in Figure 13. It can be seen from this series that the orbits retain the same general characteristics over the family, but the orbits become significantly smaller with increasing C or decreasing V_∞. A number of orbital characteristics of the orbits across the family may be computed, and some relevant related information that may be produced is shown in Figure 14. As might be expected, the V_∞ values decrease with increasing C. As the orbits become smaller with increasing C, the distance from the secondary during the flybys increases, and the orbits become correspondingly more stable. One interesting feature that corresponds to the small kink observed in Figures 14(a) and 14(d) can be observed as the orbits become smaller. The minimum periapse radius is generally increasing with increasing C, but near C $\approx$ 2.997-2.998, the minimum periapse shifts from those crossing near $x = 1$ to those crossing at the $y = 0$ line. (In other words, it shifts from those periapses in the vertical to those in the horizontal direction in Figure 13.) The minimum periapse radius from this point then decreases. The periods decrease slowly at lower C and then decrease more significantly as C approaches 3. The portion of the family shown here is stopped as the maximum eigenvalue of the monodromy matrix approaches 1 and the orbits become more stable.

While these characteristics are generally useful, the characteristic of interest for this study is the rate of change of the line of apsides. This rate computed over one period of the orbits is plotted and compared to the patched-conic predictions in Figure 15. It can be seen here that for larger V_∞ values near 3 km/s the predicted and computed values match well. As the V_∞ decreases, the values diverge significantly however. The smallest orbits in the lower V_∞ range can have a quite significant change in ω, but the orbits at this point begin to lose the characteristics seen for the majority of the family with close flybys of the secondary.

The differences between the patched-conic predictions and the CRTBP results can become significant for low V_∞ values, and they are worth exploring. Some insight can be obtained by computing the patched-conic
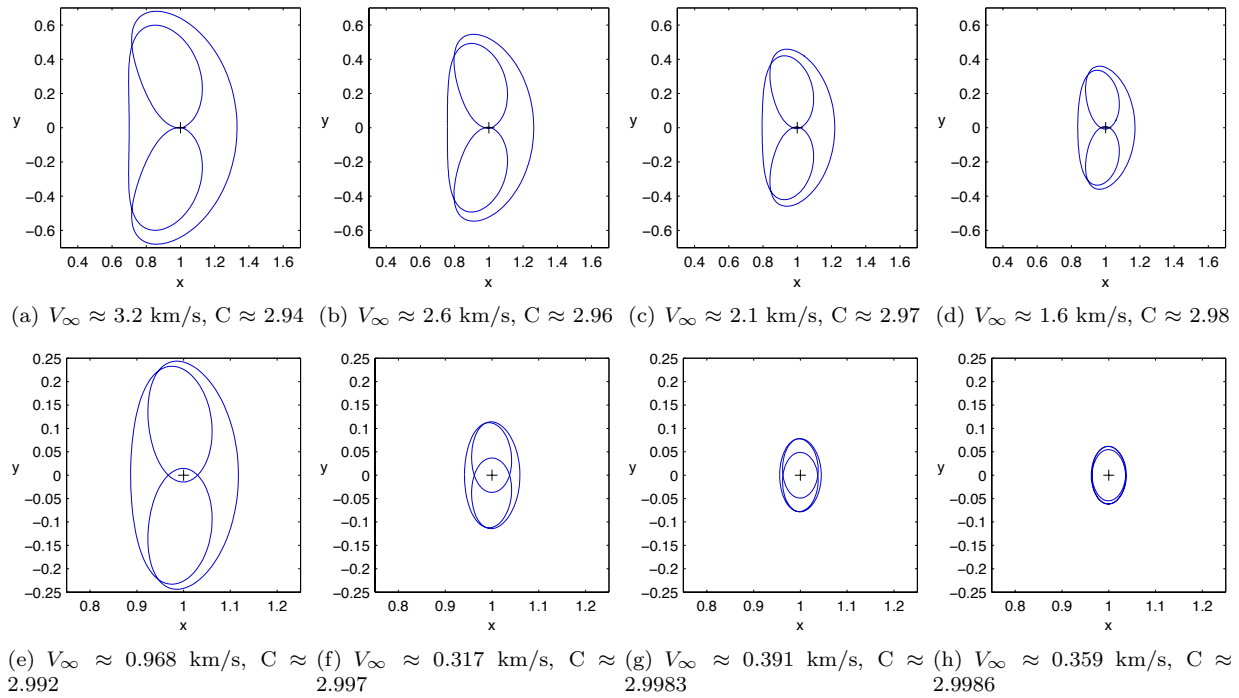
American Institute of Aeronautics and Astronautics

(a) $V_\infty \approx 3.2$ km/s, C ≈ 2.94 (b) $V_\infty \approx 2.6$ km/s, C ≈ 2.96 (c) $V_\infty \approx 2.1$ km/s, C ≈ 2.97 (d) $V_\infty \approx 1.6$ km/s, C ≈ 2.98

(e) $V_\infty \approx 0.968$ km/s, C $\approx$ (f) $V_\infty \approx 0.317$ km/s, C $\approx$ (g) $V_\infty \approx 0.391$ km/s, C $\approx$ (h) $V_\infty \approx 0.359$ km/s, C $\approx$
2.992   2.997   2.9983   2.9986

Figure 13. Selected trajectories from the Jupiter-Europa $1{:}1^+/2{:}2^-$ family.


(a)

(b)

(c)

(d)
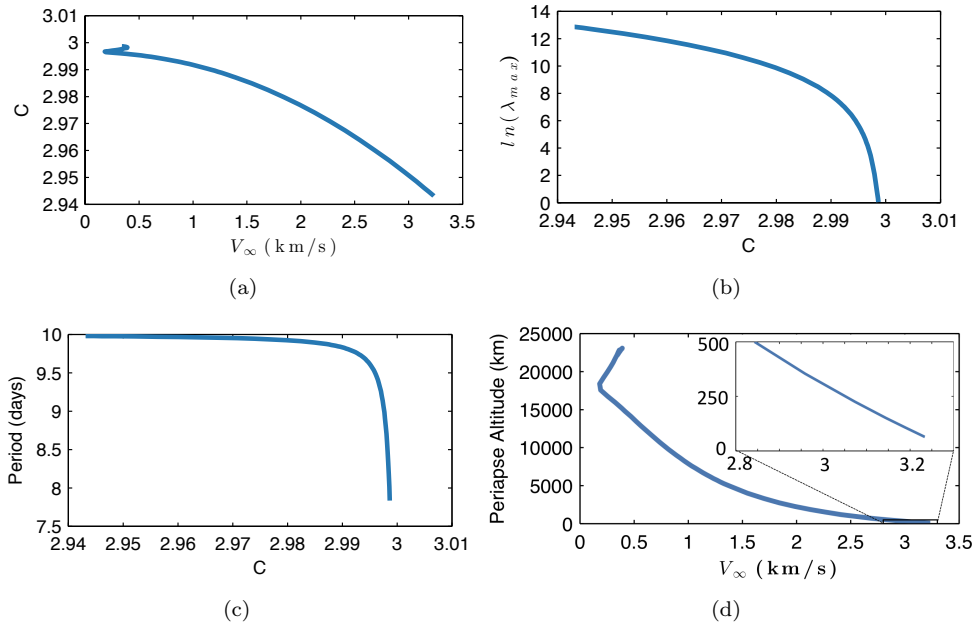
Figure 14. Characteristics of the Jupiter-Europa $1{:}1^+/2{:}2^-$ family across C and V_∞.

initial conditions at closest approach and comparing the trajectories integrated from these conditions to the orbits obtained in Figure 13. Orbits at some of these selected energies have been computed for comparison in Figure 16. In each case, the initial conditions were integrated forward and backward for half of the appropriate period to meet up with the trajectory from the other flyby. It can be seen that for higher V_∞ values, the orbit endpoints match well, and the orbit shape is similar to that obtained by conversion to a periodic orbit through differential correction. For lower V_∞ values though, the endpoints are far from each
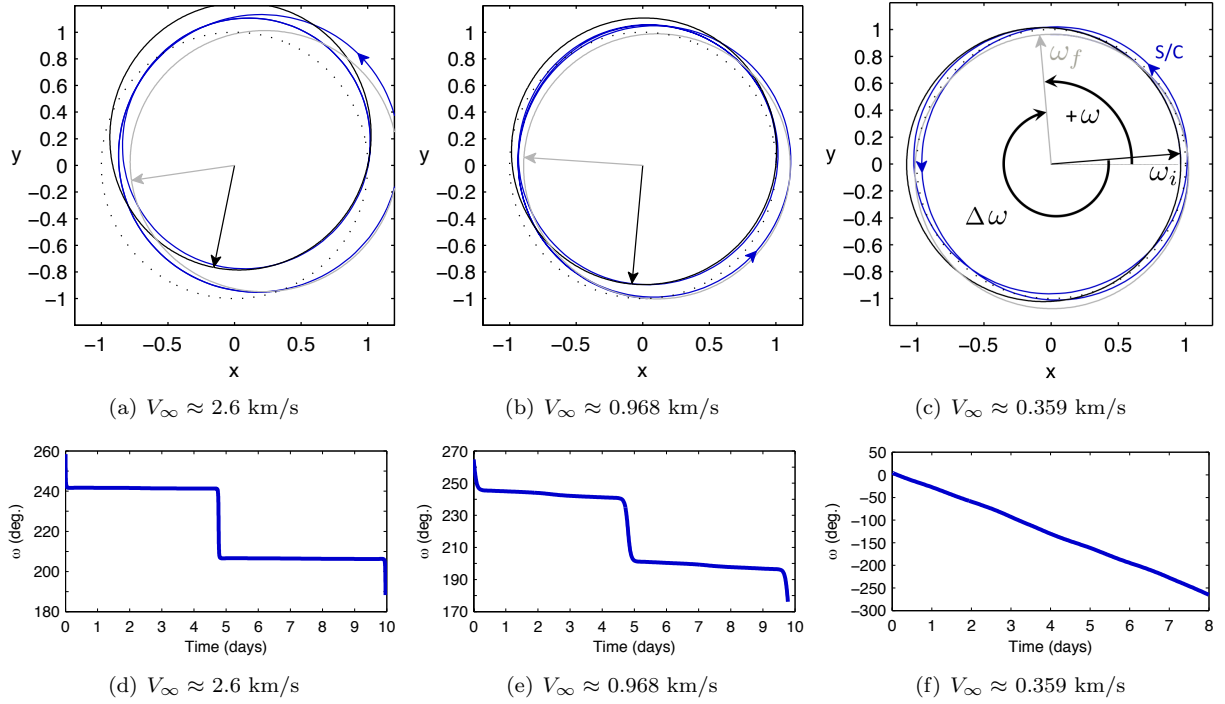
American Institute of Aeronautics and Astronautics
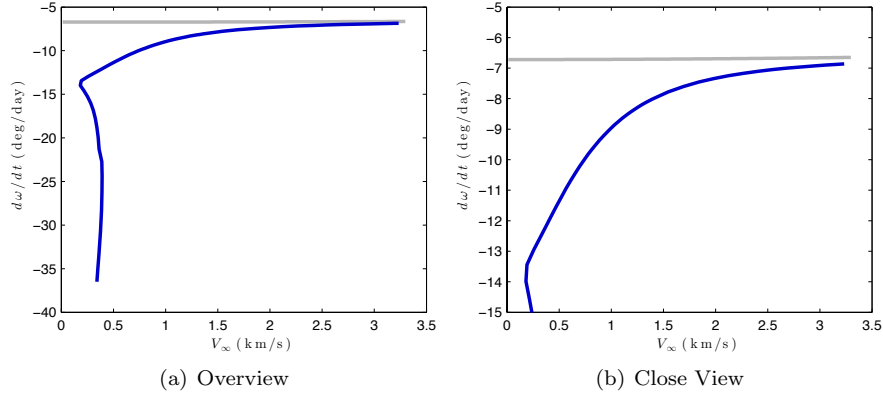
Figure 15. Comparison of the patched-conic $\dot{\omega}$ (gray) and the CRTBP $\dot{\omega}$ (blue) over a range of V_∞ values for the Jupiter-Europa $1:1^+/2:2^-$ sequence.
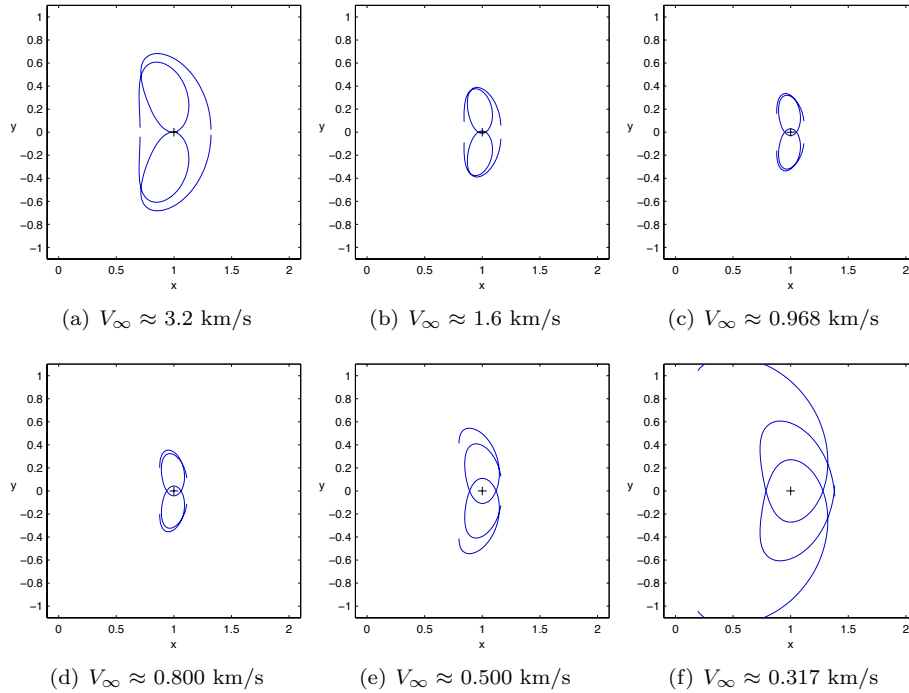
Figure 16. Selected patched-conic initial guess trajectories integrated in the CRTBP from the flybys for the Jupiter-Europa $1:1^+/2:2^-$ sequence.

other, indicating that the three-body effects are dominating, and the patched-conic prediction is no longer accurate in this region. The predicted orbit shape also diverges significantly from the orbits obtained via continuation at this point. It is at this point that the larger differences in $\dot{\omega}$ between the two models becomes most noticeable.

While the low-V_∞ cases may appear more desirable from the perspective of optimizing $\dot{\omega}$, it is useful to compare some specific cases to understand the characteristics of these orbits more fully. Plots of the orbits for several specific cases from Figure 13 in the inertial frame are given in Figure 17 along with the corresponding time histories of ω. The higher V_∞ cases behave as expected with large changes in orbital elements corresponding to the close flybys of the spacecraft with the secondary. This effect is slightly less apparent as V_∞ is reduced to approximately 1 km/s, and it is nearly gone with the lower V_∞ values. Indeed, it seems to be approaching something similar to a distant retrograde orbit (DRO) around Europa, and the stability correspondingly approaches 1.

American Institute of Aeronautics and Astronautics

(a) $V_\infty \approx 2.6$ km/s   (b) $V_\infty \approx 0.968$ km/s   (c) $V_\infty \approx 0.359$ km/s

(d) $V_\infty \approx 2.6$ km/s   (e) $V_\infty \approx 0.968$ km/s   (f) $V_\infty \approx 0.359$ km/s

Figure 17. Selected trajectories from the $1{:}1^+/2{:}2^-$ sequence Figure 13 plotted in the inertial frame. The initial and final osculating two-body orbit is plotted in black and gray, respectively. The direction of the argument of periapse is indicated with the arrows in each case.

VI.   Characteristics of Periodic Petal Rotation Trajectories in the CRTBP

The comparisons of the patched-conic and CRTBP results for the $k{:}k$ periodic orbits so far show that there can be significant differences between the $\dot{\omega}$ predicted in each case. These types of orbits may potentially be useful in tour designs and as target orbits themselves for observations of the secondary or other objects. While an exhaustive list of the characteristics of these orbits is beyond the scope of this study, representative characteristics are given here that give an indication of the results that would be expected for these types of orbits in various systems.

A.   Jupiter-Europa

A wide range of $k{:}k$ orbit combinations are possible, and several representative orbits in the Jupiter-Europa system will be described here along with their characteristics. In each case, the patched-conic initial guess is used to compute a periodic orbit in the CRTBP, and continuation is used to explore the characteristics of the family. The set of orbits computed in the CRTBP for this study is shown in Figure 18. Each orbit possesses two flybys with multiple loops around the secondary that correspond to the chosen resonance. By comparing the $1{:}1^+/2{:}2^-$ case and the $4{:}4^+/4{:}4^-$ case it can be seen that the orbits become significantly more complicated with corresponding increases in the period of the orbit. The close flybys at high energies (low C) make them generally unstable.

The characteristics of the families for each of these orbits may be computed in a manner similar to that described earlier for the $1{:}1^+/2{:}2^-$ case, and $\dot{\omega}$ in particular may also be found for each family as a function of various parameters. The values of $\dot{\omega}$ as a function of V_∞ are plotted for each continued family in Figure 19(b) and compared to the patched-conic predictions for each case in Figure 19(a). As was seen for the initial case computed in the Jupiter-Europa system, the $\dot{\omega}$ values match well for higher V_∞, but the lower V_∞ cases can diverge from the patched-conic predicted values significantly in each case. The $1{:}1^+/2{:}2^-$ case does give the greatest difference over time, but it should be remembered that this difference corresponds to those orbits essentially orbiting the secondary at a distance.
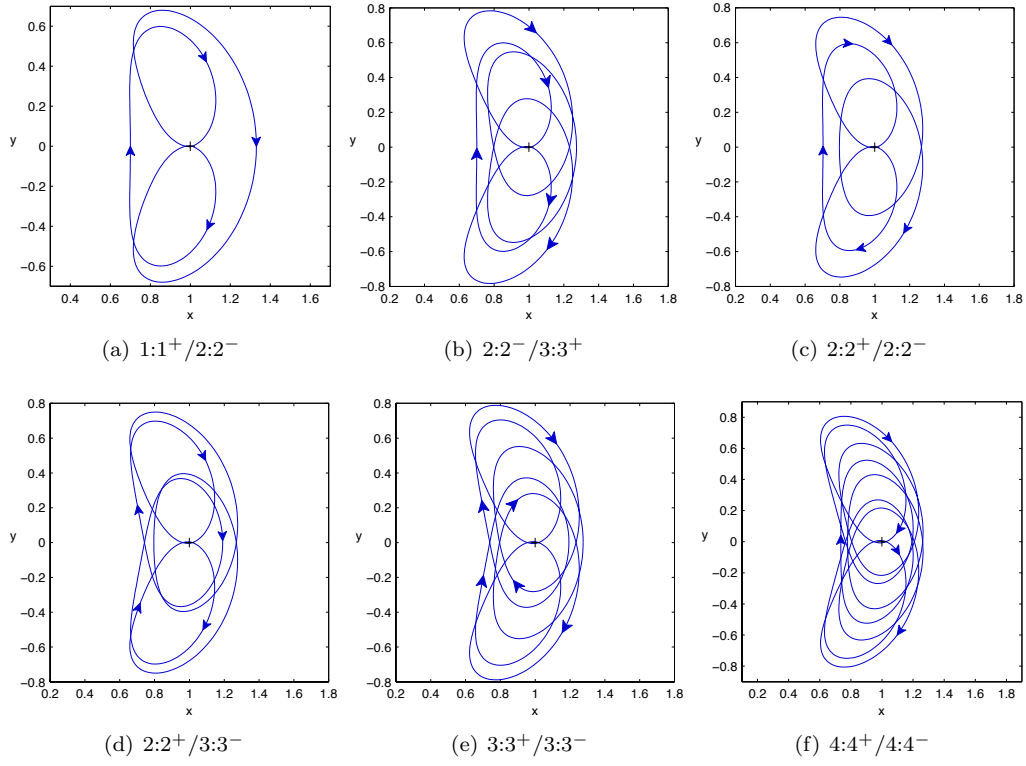
(a) 1:1$^+$/2:2$^-$ (b) 2:2$^-$/3:3$^+$ (c) 2:2$^+$/2:2$^-$

(d) 2:2$^+$/3:3$^-$ (e) 3:3$^+$/3:3$^-$ (f) 4:4$^+$/4:4$^-$

Figure 18. Sample of Jupiter-Europa petal rotation trajectories for various non-resonant orbits in the CRTBP.
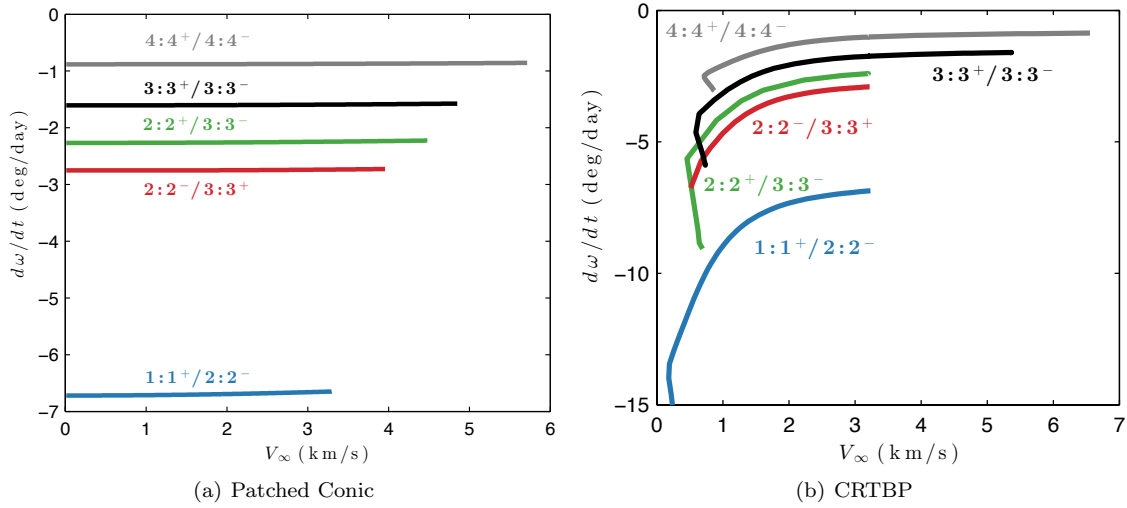

(a) Patched Conic   (b) CRTBP

Figure 19. Patched-conic predictions and CRTBP results for $\dot{w}$ in the Jupiter-Europa system for selected k:k orbits. Note the difference in the scales of the axes.
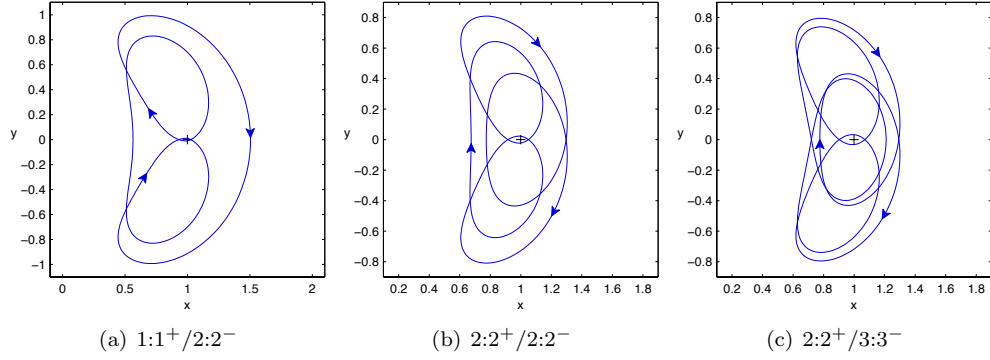
B. Saturn-Titan

A similar analysis to that performed for Jupiter-Europa is performed here for the Saturn-Titan system. Referring back to Table 1 shows that the mass ratio of the Saturn-Titan system is at the other end of the spectrum for the systems of interest here. These plots show a number of differences, primarily in the magnitude of the quantities of interest from which the characteristics of the other systems may be inferred.

In Figure 20 an overview of some of the trajectories computed for the Saturn-Titan system is given. They generally have similar features as those seen in the Jupiter-Europa system, but of course some of the

American Institute of Aeronautics and Astronautics

characteristics at each energy vary. A sample of some selected orbits from the continuation process for the $1:1^+/2:2^-$ orbit is given in Figure 21. Some of the larger orbits vary from those seen in the Jupiter-Europa

(a) $1:1^+/2:2^-$ (b) $2:2^+/2:2^-$ (c) $2:2^+/3:3^-$

Figure 20. Sample of Saturn-Titan petal rotation trajectories for various non-resonant orbits in the CRTBP.

(a) C ≈ 2.429   (b) C ≈ 2.668   (c) C ≈ 2.805   (d) C ≈ 2.886

(e) C ≈ 2.961   (f) C ≈ 2.980   (g) C ≈ 2.990   (h) C ≈ 2.993
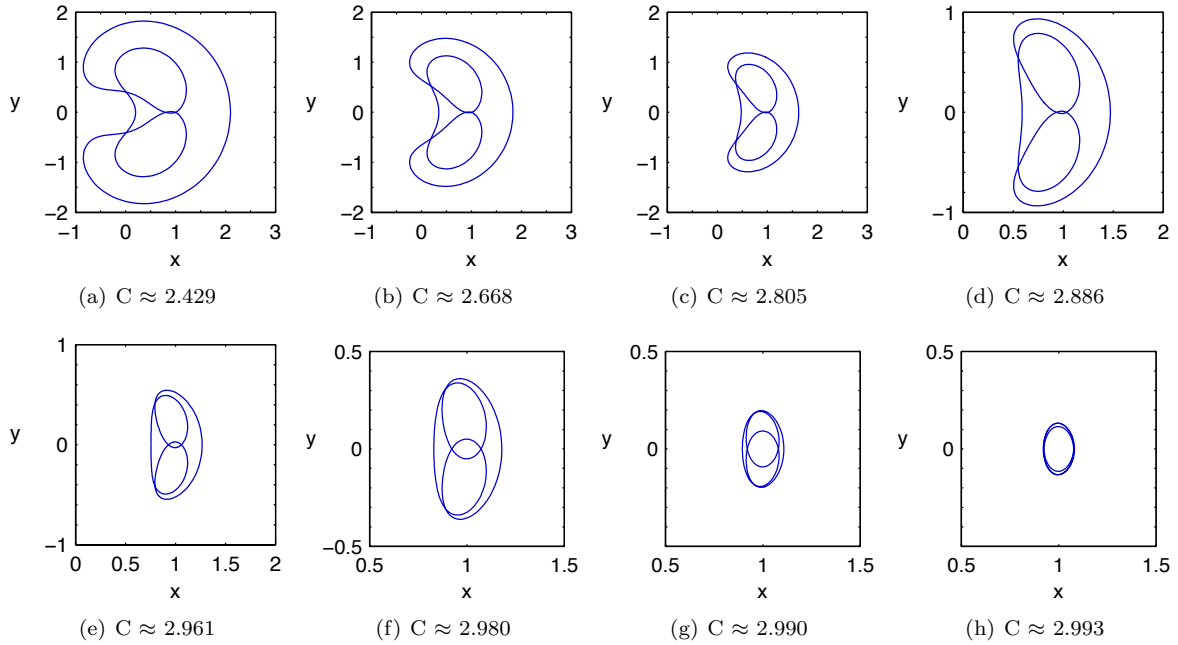
Figure 21. Sample of Saturn-Titan petal rotation trajectories across the continuation process for various $1:1^+/2:2^-$ orbits in the CRTBP.

system, but the qualitative nature of the family through the continuation is the same. A comparison of $\dot{\omega}$ for the continued families of orbits with the patched-conic predictions is given in Figure 22. Characteristics similar to the comparison in the Jupiter-Europa system are seen here. The predicted magnitude of $\dot{\omega}$ is smaller, and the CRTBP results are correspondingly smaller. They again match the predicted results best at the higher V_∞ ranges. In this case the deviation in $\dot{\omega}$ is greatest below approximately 1.5 km/s.

C. Galilean Moons & Neptune-Triton

Many of the features and expected trends of the systems in Table 1 may be deduced or extrapolated from the results given so far for the Jupiter-Europa and Saturn-Titan systems. The converged orbits for the same sequences in each look similar to those computed so far, although they will of course vary at each particular energy. A sample of some of the orbits computed in each system is given in Figure 23. Further insights into the differences seen in each system may be obtained by comparing parameters such as $\dot{\omega}$ in Figure 24. Comparing these plots shows that Jupiter-Io and Jupiter-Europa generally have the greatest rate
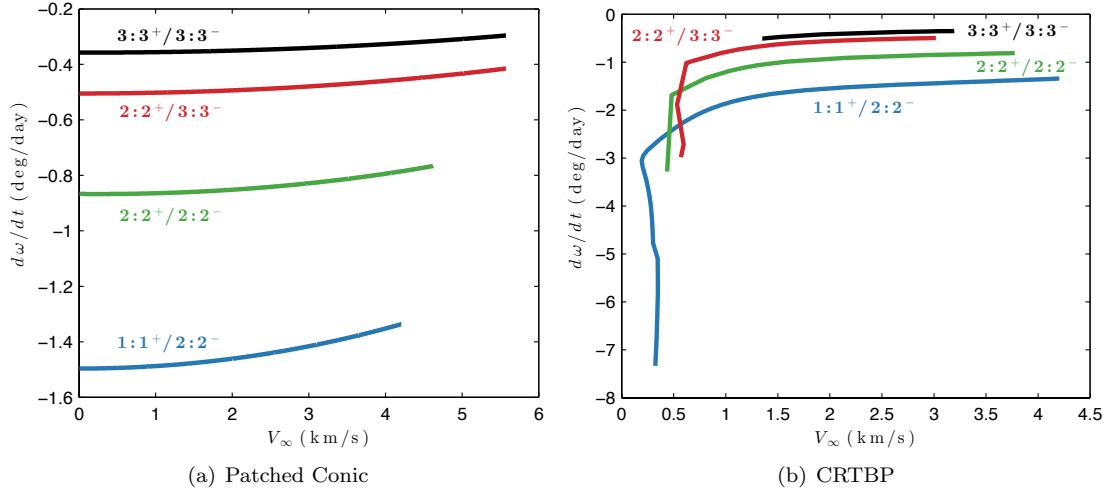
American Institute of Aeronautics and Astronautics

(a) Patched Conic

(b) CRTBP

Figure 22. Patched-conic predictions and CRTBP results for $\dot{w}$ in the Saturn-Titan system.

(a) Jupiter-Io $1{:}1^+/2{:}2^-$ (b) Jupiter-Gany. $2{:}2^+/2{:}2^-$ (c) Jupiter-Callisto $2{:}2^+/3{:}3^-$ (d) Nept.-Triton $2{:}2^+/3{:}3^-$
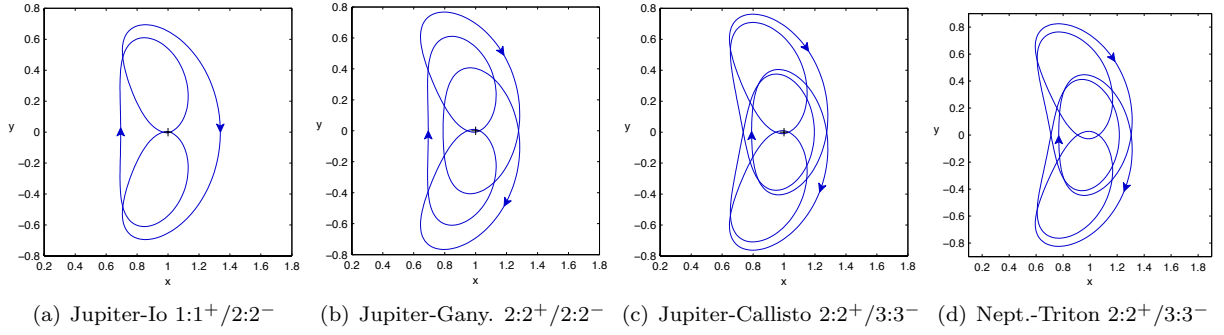
Figure 23. Sample of petal rotation trajectories for various non-resonant orbits and systems in the CRTBP.

of change for this case. The pairs Neptune-Triton/Jupiter-Ganymede and Saturn-Titan/Jupiter-Callisto are both surprisingly similar at least over a portion of the V_∞ range. The larger negative trends seen in $\dot{\omega}$ occur below approximately 3 km for the Jupiter-Io system moving up to below approximately 1.5 km/s in the
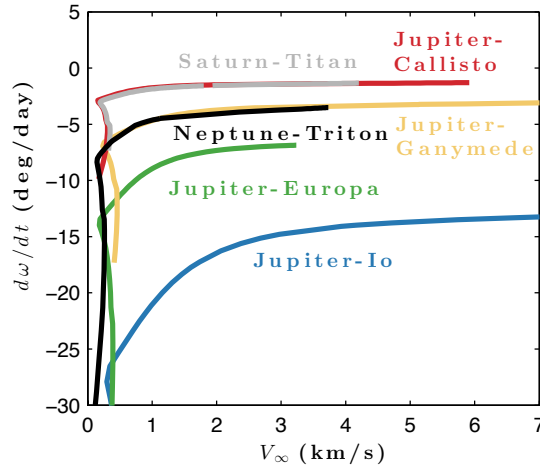

Figure 24. $\dot{\omega}$ for the $1{:}1^+/2{:}2^-$ case in the chosen systems.

American Institute of Aeronautics and Astronautics

Saturn-Titan and Jupiter-Callisto systems. Qualitatively similar differences with the patched-conic results may be found for each system as well.

VII.   Conclusions

Patched-conic solutions can be used to provide a quick method of evaluating the tour design space for available trajectories with desired rates of $\dot{\omega}$. They also provide a sufficiently accurate approximation at higher energies to allow the convergence of corresponding orbits in the CRTBP and their continuation to lower energies. At lower energies, particular cases appear to approach orbits similar to DROs. For trajectories that generally stay far from the secondary such as the $1:4^+/1:5^-$ sequence, the patched-conic and CRTBP results matched well over the majority of the V_∞ values, but some differences were noted even there for the lower range of V_∞. These types of differences are worth noting and have the potential to be significant for particular non-resonant orbit sequences. For trajectories that are closer to the secondary's orbit, significant differences in $\dot{\omega}$ may be found with lower V_∞. For systems such as Jupiter-Europa these differences could be found below approximately 3 km/s V_∞ values, and below approximately 1.5 km/s V_∞ values for Saturn-Titan. These differences are important at these lower energies, and the provided rates can provide a guideline for extended mission or endgame design scenarios.

VIII.   Future Work

Future work will include the analysis of additional orbit sequences in these systems as well as others. Preliminary analysis indicates that the invariant manifolds and heteroclinic connections possible with these orbits can provide useful transfers, and these transfers will be analyzed in the future.

Acknowledgements

References

[1]Peralta, F. and Flanagan, S., "Cassini Interplanetary Trajectory Design," *Control Engineering Practice*, Vol. 3, No. 11, 1995, pp. 1603–1610.

[2]Smith, J. C., "Description of Three Candidate Cassini Satellite Tours," *Spaceflight Mechanics: Proceedings of the Spaceflight Mechanics Conference held February 9-11, 1998 in Monterey, California*, edited by J. W. Middour, L. L. Sackett, L. A. D'Amario, and D. V. Byrnes, Vol. 99 of *Advances in the Astronautical Sciences*, American Astronautical Society, Univelt Inc., San Diego, California, 1998.

[3]Wolf, A. and Smith, J., "Design of the Cassini Tour Trajectory in the Saturnian System," *Control Engineering Practice*, Vol. 3, No. 11, 1995, pp. 1611–1619.

[4]Buffington, B., Strange, N. J., and Smith, J., "Overview of the Cassini Extended Mission Trajectory," *AIAA/AAS Astrodynamics Specialist Conference*, No. Paper 2008-6752, Honolulu, Hawaii, August 18-21 2008.

[5]Smith, J. and Buffington, B., "Overview of the Cassini Solstice Mission Trajectory," *AAS/AIAA Astrodynamics Conference*, Pittsburgh, Pennsylvania, August 2009, pp. AAS 09–351.

[6]Buffington, B., Campagnola, S., and Petropoulos, A. E., "Europa Multiple Flyby Trajectory Design," *AIAA/AAS Astrodynamics Specialists Conference*, No. AIAA 2012-5069, Minneapolis, Minnesota, August 13-16 2012.

[7]Campagnola, S., Buffington, B. B., and Petropoulos, A. E., "Jovian Tour Design for Orbiter and Lander Missions to Europa," *Acta Astronautica*, Vol. 100, 2014, pp. 68–81.

[8]Buffington, B., "Trajectory Design for the Europa Clipper Mission Concept," *2014 AIAA/AAS Astrodynamics Specialists Conference*, San Diego, California, August 4-8 2014.

[9]Campagnola, S., Boutonnet, A., Martens, W., and Masters, A., "Mission Design for the Exploration of Neptune and Triton," *IEEE Aerospace and Electronics Systems Magazine*, (submitted).

[10]Masters, A., Achilleos, N., Agnor, C., Campagnola, S., Charnoz, S., Christophe, B., Coates, A. J., Fletcher, L. N., G. H. Jones, L. L., Marzari, F., Nettelmann, N., Ruiz, J., Ambrosi, R., Andre, N., Bhardwaj, A., Fortney, J. J., Hansen, C. J., Helled, R., Moragas-Klostermeyer, G., Orton, G., Ray, L., Reynaud, S., N. Sergis, R. S., and Volwerk, M., "Neptune and Triton: Essential Pieces of the Solar System Puzzle," *Planetary and Space Science*, 2014.

[11]Boutonnet, A. and Schoenmaekers, J., "Mission Analysis for the JUICE Mission," *Space Flight Mechanics: Proceedings of the AAS/AIAA 22nd Space Flight Mechanics Meeting held January 29 - February 2, 2012 in Charleston, South Carolina*, edited by J. V. McAdams, D. P. McKinley, M. M. Berry, and K. L. Jenkins, Vol. 143 of *Advances in the Astronautical Sciences*, American Astronautical Society, Univelt Inc., San Diego, California, 2012, pp. 1561–1578.

[12]Langevin, Y., "Mission Design Issues for the European Orbiter of Laplace/EJSM: Calisto Flybys Sequence," *Proceedings of the AAS/AIAA Astrodynamics Specialist Conference*, Vol. 135, Pittsburgh, Pennsylvania, August 9-13 2009, pp. 967–986.

[13]Russell, R. P. and Strange, N. J., "Cycler Trajectories in Planetary Moon Systems," *Journal of Guidance, Control, and Dynamics*, Vol. 32, No. 1, January - February 2009, pp. 143–157.

[14]Murray, C. D. and Dermott, S. F., *Solar System Dynamics*, Cambridge University Press, Cambridge, United Kingdom, 1999, pp. 421-428.

[15]Koon, W. S., Lo, M. W., Marsden, J. E., and Ross, S. D., "Resonance and Capture of Jupiter Comets," *Celestial Mechanics and Dynamical Astronomy*, Vol. 81, No. 1-2, 2001, pp. 27–38.

[16]Barrabés, E. and Gómez, G., "Spatial p-q Resonant Orbits of the RTBP," *Celestial Mechanics and Dynamical Astronomy*, Vol. 84, 2002, pp. 387–407.

[17]Anderson, R. L., "Approaching Moons from Resonance via Invariant Manifolds," *22nd AAS/AIAA Space Flight Mechanics Meeting*, No. AAS 12-136, Charleston, South Carolina, January 29 - February 2 2012.

[18]Campagnola, S. and Russell, R., "Endgame Problem Part 1: V-Infinity-Leveraging Technique and the Leveraging Graph," *Journal of Guidance, Control, and Dynamics*, Vol. 33, No. 2, 2010, pp. 463–475.

[19]Marchand, B. G., Howell, K. C., and Wilson, R. S., "Improved Corrections Process for Constrained Trajectory Design in the n-Body Problem," *Journal of Spacecraft and Rockets*, Vol. 44, No. 4, July-August 2007, pp. 884–894.

[20]Anderson, R. L., Campagnola, S., and Lantoine, G., "Broad Search for Unstable Resonant Orbits in the Planar Circular Restricted Three-Body Problem," *AAS/AAIA Astrodynamics Specialist Conference*, No. AAS 13-787, Hilton Head Island, South Carolina, August 11-15 2013.

[21]Anderson, R. L., *Low Thrust Trajectory Design for Resonant Flybys and Captures Using Invariant Manifolds*, Ph.D. thesis, University of Colorado at Boulder, 2005.

[22]Anderson, R. L. and Lo, M. W., "Role of Invariant Manifolds in Low-Thrust Trajectory Design," *Journal of Guidance, Control, and Dynamics*, Vol. 32, No. 6, November-December 2009, pp. 1921–1930.

[23]Anderson, R. L. and Lo, M. W., "Dynamical Systems Analysis of Planetary Flybys and Approach: Planar Europa Orbiter," *Journal of Guidance, Control, and Dynamics*, Vol. 33, No. 6, November-December 2010, pp. 1899–1912.

[24]Anderson, R. L. and Lo, M. W., "A Dynamical Systems Analysis of Planetary Flybys and Approach: Ballistic Case," *The Journal of the Astronautical Sciences*, Vol. 58, No. 2, April-June 2011, pp. 167–194.

[25]Anderson, R. L. and Lo, M. W., "Flyby Design using Heteroclinic and Homoclinic Connections of Unstable Resonant Orbits," *Spaceflight Mechanics: Proceedings of the 21st AAS/AIAA Space Flight Mechanics Meeting held February 13-17, 2011, New Orleans, Louisiana*, edited by M. K. Jah, Y. Guo, A. L. Bowes, and P. C. Lai, Vol. 140 of *Advances in the Astronautical Sciences*, American Astronautical Society, Univelt Inc., San Diego, California, 2011, pp. 321–340.

[26]Anderson, R. L., "Approaching Moons from Resonance via Invariant Manifolds," *Journal of Guidance, Control, and Dynamics*, 2014 (in press).

[27]Uphoff, C., Roberts, P. H., and Friedman, L. D., "Orbit Design Concepts for Jupiter Orbiter Missions," *Journal of Spacecraft and Rockets*, Vol. 13, No. 6, 1976, pp. 348–355.

[28]Strange, N. J. and Sims, J. A., "Methods for the Design of V-Infinity Leveraging Maneuvers," *Astrodynamics: Proceedings of the AAS/AIAA Astrodynamics Conference, July 30 - August 2, 2001, Quebec City, Quebec*, edited by D. B. Spencer, C. C. Seybold, A. K. Misra, and R. J. Lisowski, Vol. 109 of *Advances in the Astronautical Sciences*, American Astronautical Society, Univelt Inc., San Diego, California, 2001.

[29]Campagnola, S., Strange, N., and Russell, R., "A Fast Tour Design Method using Non-Tangent V-Infinity Leveraging Transfer," *Celestial Mechanics and Dynamical Astronomy*, Vol. 108, 2010, pp. 165–186.

[30]Campagnola, S., Skerritt, P., and Russell, R. P., "Flybys in the Planar, Circular, Restricted, Three-Body Problem," *Celestial Mechanics and Dynamical Astronomy*, Vol. 113, No. 3, 2012, pp. 343–368.

[31]Strange, N., Russell, R., and Buffington, B., "Mapping the V-Infinity Globe," *Astrodynamics: Proceedings of the AAS/AIAA Astrodynamics Conference held August 19-23, 2007, Mackinac Island, Michigan*, edited by R. J. Proulx, J. Thomas F. Starchville, R. D. Burns, and D. J. Scheeres, Vol. 129 of *Advances in the Astronautical Sciences*, American Astronautical Society, Univelt Inc., San Diego, California, 2007.

[32]Szebehely, V., *Theory of Orbits: The Restricted Problem of Three Bodies*, Academic Press, New York, 1967.

[33]Buffington, B., Strange, N., and Campagnols, S., "Global Moon Coverage Via Hyperbolic Flybys," *23rd International Symposium on Space Flight Dynamics*, Pasadena, California, October 29 - November 2 2012.

[34]Wilson, R. S., "Derivation of Differential Correctors Used in GENESIS Mission Design," IOM 312.I-03-002, Jet Propulsion Laboratory, 2003.

[35]Marchand, B., Howell, K. C., and Wilson, R., "An Improved Corrections Process for Constrained Trajectory Design in the n-Body Problem," *Journal of Spacecraft and Rockets*, Vol. 44, No. 4, 2007, pp. 884–897.

[36]Parker, J. S. and Anderson, R. L., *Low-Energy Lunar Trajectory Design*, Vol. 12 of *JPL Deep Space Communications and Navigation Series*, John Wiley & Sons, Inc., Hoboken, New Jersey, 1st ed., June 2014.

[37]Howell, K. C. and Breakwell, J. V., "Three-Dimensional, Periodic, 'Halo' Orbits," *Celestial Mechanics*, Vol. 32, No. 1, January 1984, pp. 53–71.

[38]Gómez, G., Llibre, J., R., M., and Simó, C., *Dynamics and Mission Design Near Libration Points Vol. I Fundamentals: The Case of Collinear Libration Points*, Vol. 2 of *World Scientific Monograph Series in Mathematics*, World Sci., NJ, 2001.

[39]Dichmann, D. J., Doedel, E. J., and Paffenroth, R. C., "The Computation of Periodic Solutions of the 3-Body Problem Using the Numerical Continuation Software AUTO," *International Conference on Libration Point Orbits and Applications*, Aiguablava, Spain, June 10-14 2002.